GeoConvention
Calgary • Canada • March 7-11 2016
OPTIMIZING RESOURCES

Hydro-mechanical Modelling of Fault Movement in Response to Subsurface Fluid Injection, a Finite Element Approach

Luyi Shen[1] and Douglas R. Schmitt[2]
[1]Alberta Geological Survey, Alberta Energy Regulator
[2]Department of Physics, University of Alberta

Summary

There is a general consensus that pressurized injection of fluid has the potential to trigger slip on properly oriented faults. Seismicity induced by such events has been observed during well-stimulation activities for geothermal and hydrocarbon energy exploration and development operations. While we believe we have a good understanding of the basic mechanics associated with fault movement the details remain unknown. This study investigates potential mechanisms producing fluid pressure induced fault movement through a fully coupled hydro-mechanical modelling approach on a simplified fault system. The model also incorporates a dynamic frictional model that adjusts friction depending on motion. The modelling results indicate that the history of slip on the fault depends not just on the injection pressure but that changing the pressurization duration and the timing of the well shut-in may also play key roles. By testing how faults with different geomechanical properties respond to different hydraulic loadings, we demonstrate the importance of using a coupled hydro-mechnical model and highlight that detailed knowledge of the geomechanical properties of the fault of interest is needed to further improve our understanding of hydraulically-driven fault slippage.

Introduction

Researchers have hypothesized that fluid injected into the subsurface can potentially flow into faults and, in certain situations, can lead to fault slippage due to a reduction in effective confining stress and shear friction (see review in Schmitt, 2014). Although such a theory, incorporated with Coulomb friction theory provides a basic explanation for the occurrence of fluid injection induced earthquakes (Griggs and Handin, 1960, Harris and Simpson, 1998), more geometrically specific numerical simulations are required to quantify the displacements and timing of fault movements in more geologically realistic situations (Baisch et al., 2010, Rutqvist et al., 2013, Zhao et al., 2009). Knowledge of these parameters translates directly to a precise estimate of magnitudes of the seismicity. Further, any fluid flow associated with the fault movement and the related poro-elastic deformation of the surrounding rock mass, components which are often not considered, can only be computed with numerical modelling.

For this study, we built a fully coupled hydro-mechanical Finite Element model that incorporates a hypothetical fault to study fault slip in response to adjacent fluid pressurization and flow. The shear friction stresses, contact stresses, pore pressure propagation, and slip displacement are carefully investigated to provide an understanding of fault movement as a result of the perturbation of the in-situ stress in response to subsurface fluid flow.

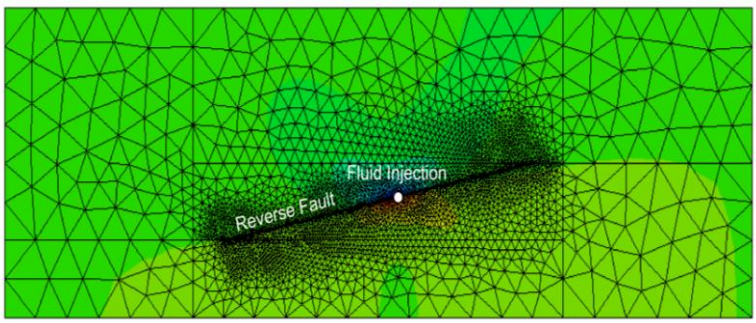

Figure 1. A snapshot of the Finite Element model utilized in this study. Higher density grids near the fault line are used for better prediction of fault behaviour in this simulation. The fluid injection point is placed in the middle of the fault. The different colours on the two sides of the fault indicate the magnitude of induced slip.

Theory and/or Method

A 2D simplified model consisting of an initially uniform rock mass containing a reverse fault was constructed (Figure 1). Inclusion of an

actual fault can be problematic as its thickness is often very small relative to the overall dimensions of the model. Here, we overcome this limitation by representing the fault as two separable surfaces with modifiable frictional and hydraulic properties. Some generic assumptions about the geomechanical properties of this model were made for this preliminary research to test the concept of fully coupled transient hydro-mechanical simulation. We configured the model with a depth of 8000 m and a width of 24000 m. A 'fault' with a length of 10000 m and slanted at an angle of ~78° from vertical was placed in the lower half of the model between 4000 m and 6000 m depth. An initial in-situ stress S_h/S_v ratio of 2 was applied with the intent to represent a reverse fault close to critical state. In this initial model, we surrounded the fault with a low permeability rock mass in order to focus fluid flow into and along the higher permeability fault. This might represent a newly developing fault prior to the development of a clay gouge. We calculated the evolving permeability of the fault material using the Kozeny-Carman equation (Carman, 1956) assuming an initial permeability of 100 μDarcy with the porosity perturbation computed through a poro-elastic theory approach. In the future we will incorporate a more advanced fracture permeability model (i.e., the Barton-Bandis Model (Barton et al., 1985)).

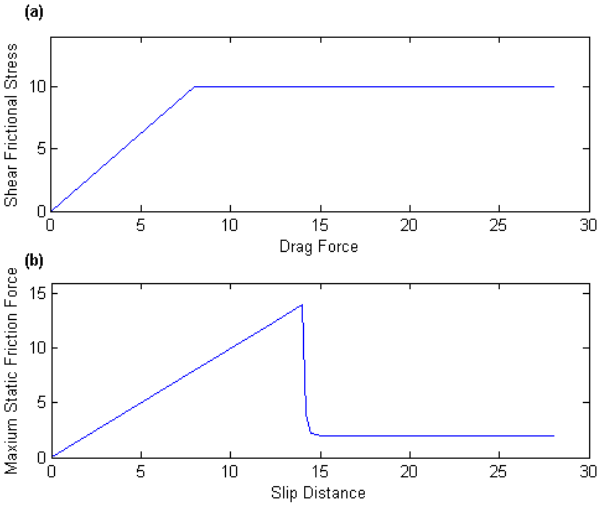

Figure 2. Conceptual illustration of the frictional behaviours of fault. a) The shear frictional force change in response to increasing drag force. b) The relationship between maximum static frictional force and fault-slip distance under constant contact pressure

A stick-slip paradigm is employed in the modelling (Brace and Byerlee, 1966). Under progressive external loading, the formation surrounding the fault first experiences recoverable elastic deformation (pre-slip elastic displacement). Once the deformation reaches a threshold, the fault ruptures commencing irreversible non-elastic displacement. A simple illustration for the relationship between relative movement of two sides of a fault and maximum shear frictional stress is shown in Figure 2. In the initial elastic deformation (stick) phase, the maximum shear friction stress increases proportionally as the two sides of the fault are displaced relative to each other until a threshold pre-slip elastic displacement distance is reached (Figure 2b). Once sliding commences, the maximum shear frictional stress is usually governed by the friction coefficient and contact pressure of the fault. The friction coefficient, which determines the ratio between contact pressure and maximum shear frictional stress, is usually slip-rate dependent. The static frictional coefficient (which is most dominant when the fault is sticking or slowly creeping) is usually much higher than its kinetic counterpart (Martins et al., 1990). Figure 2a shows the relationship between maximum shear frictional stress and drag force under constant contact pressure. Initially, the shear frictional stress increases along with increasing drag force to prevent fault movement (or to only allow the fault to creep). Once the drag force is sufficient to induce slip of the fault, the maximum shear friction drops dramatically and induces further fault movement.

Assuming the fault is connected with a reservoir targeted by a hydraulic fracturing operation through a fluid passage, the fluid pressure at the both ends of the passage should be well correlated. The model is then perturbed further by the application of a point fluid source on the fault that remains at constant pressure. In this study, we assume a point in our model to be one end of the fluid passage and enforce a boundary condition of changing hydraulic pressure (see Figure 3b) at that point (see Figure 1). Such an approach allows us to reasonably estimate the fluid pressure change in the fault in response to the pressure change in the reservoir pressure. In contrast, enforcing a constant fluid flow will result in inaccurate estimation of pore pressure of the fault does not follow linearly with the hydraulic with the hydraulic loading. Due to the application of the stick-slip model and the dynamic frictional coefficient, the maximum shear frictional stress will vary depending on the current stress state but also on the relative movement of the fault computed from previous stress states. Therefore it is plausible to suspect that a slight change in the magnitude and timing of the hydraulic loading may result in very different fault movement behaviour. More testing

regarding this issue will be shown in the text below. It is also worth noting that the pressure loading used in this preliminary study is ad hoc and does not necessarily reflect real situations. Future analyses will allow for more realistic pressurization time series to be applied.

Examples

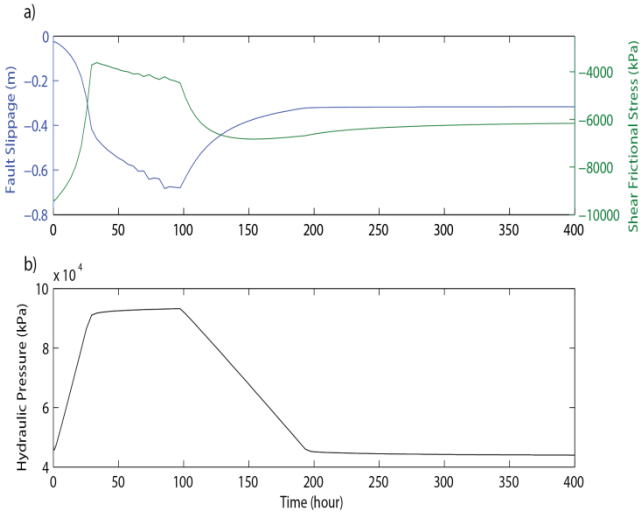

Figure 3. Fault slippage results of the first simulation. a) Maximum fault movement (left Y-axis) and the corresponding shear frictional stress (right Y-axis). b) Fluid pressure at the point of maxium slippage during the simulation.

Figure 3 shows the result of our first simulation. The fluid is injected into the fault by increasing hydraulic pressure at an arbitary point near the fault. The pressure is increased from its normal hydrostatic value to a maximum of ~9000 kPa and is held stable for ~80th hours. At ~100th hours, the fluid pressure is allowed to decline until it reaches its initial hydrostatic value near ~200th hours after which it is held constant for the rest of the simulation. We applied this fluid pressure variation to provide an analogy for possible fluid leakage from reservoirs undergoing hydraulic fracturing. The fluid pressure increase in the first stage represents the fracturing stage. During the shut-in stage, the fluid pressure remains relatively stable and then decreases when the production stage starts.

Figure 3a shows the maximum relative movement of two sides of the fault and the shear frictional stress at the point with the maximum relative displacement. The two sides of the fault start moving in opposite directions. Simultaneously with the increasing fluid pressure, the contact pressure drops resulting in lower maximum shear friction stress. The fault movement accelerates with decreasing shear frictional stress between the ~10th and the ~40th hour. After the fluid pressure has reached its maximum value, the fault continues to move but at lower rate due to increasing shear friction stress. At ~100th hours, the fault slip reaches a maximum of 0.7 m. After the shut-in stage, the fault recovers some of this displacement as the stresses revert back to their initial state. But, due to the non-recoverable fricitonal slip and changing friction coefficient, only a portion of the displacement is recovered. It is worth noting that the “recoverable slip” in this simulation is not necessarily elastic slip. Reducing the hydraulic pressure to the initial hydrostatic value would be inclined to reverse the stress state back to its initial condition as well. Although facing the resistance of the shear frictional force, such change in the stress state will tend to move the two sides of the fault back to their initial positions.

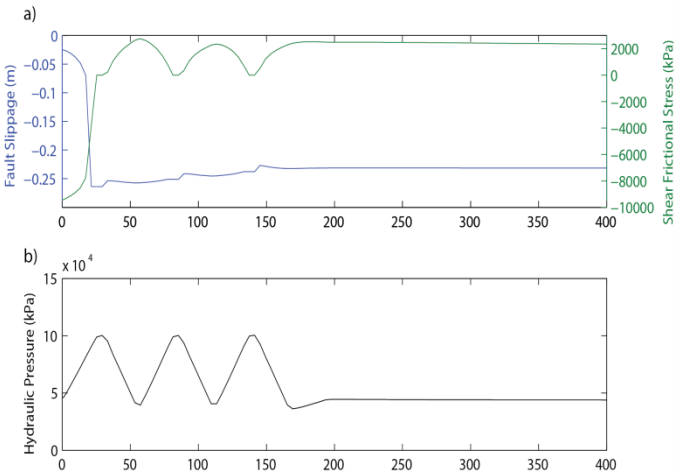

Figure 4. Fault slippage results of the second simulation. a) Maximum fault movement (left Y-axis) and the corresponding shear frictional stress (right Y-axis). b) Fluid pressure at the point of maximum slippage during the simulation.

It was suggested that changing the hydraulic loading conditions will result in different patterns of displacement. Our second simulation was designed to model the impact of cyclic hydraulic loading on fault movement. As shown in Figure 4b, the fluid pressure increases from the in-situ value to reach the first maximum of about 10000 kPa at ~30th hours whereupon it declines back to the initial in-situ value at ~55th hours. This pressurization pattern was repeated for 3 cycles, intended toprovide an analogy to cyclic hydraulic fracturing treatments. Fault movement and stress changes in reponse to the cyclic hydraulic loading are shown in Figure 4a. In the first

treatment cycle, fault slip started in response to the increased fluid pressure. This slip ended with cessation of pressurization but in this case the recovery of displacement is quite small. In the later cycles, alhough there is still fluctuation in the shear frictional stress, the fault slippage is very small, presumably due to the fact that the fault is only allowed to slip this far under the specified kinetic frictional coefficient. The later treatment cycle cannot induce the fault to reach the slip rate needed to move both sides of the fault further away from each other. Although the maximum fluid pressure is higher than in the first simulation (Figure 3), the maximum slippage is much smaller in this case (~0.3 m) compared to that of the previous example (~0.7 m). It is plausible that in the first simulation, the pore pressure propagates further in the fault resulting in the decrease of shear frictional stress along larger parts of the fault and, consequently, longer slip distances. Also, when the fluid pressure in the injection point is decreasing, fluid pressure in the other parts of the fault is not decreasing instantly. The remaining fluid in the fault allows the two sides of the fault to move back freely until the fluid pressure is too low and frictional force is too big. In this study, the two sides of the fault remain at the maximum ~0.3 m slippage distance from their original position.

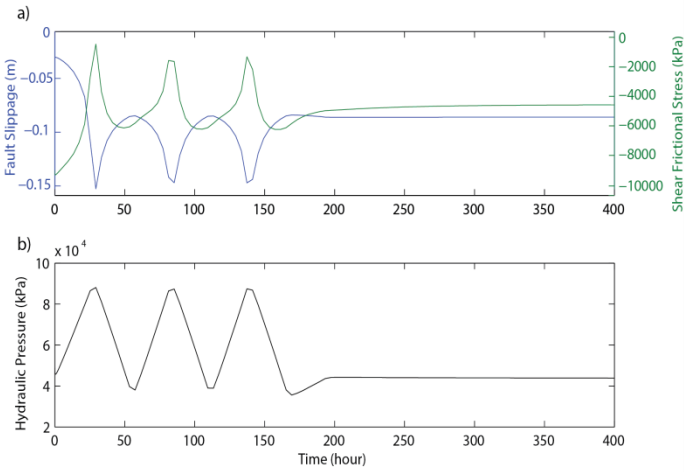

Figure 5. Fault slippage results of the third simulation. a) Maximum fault movement (left Y-axis) and the corresponding shear frictional stress (right Y-axis). b) Fluid pressure at the point of maximum slippage during the simulation.

In our third simulation, we increased the static frictional coefficient from 0.6 to 0.8 and reduced the amplitude of cyclic fluid pressure loading to 9000 kPa (Figure 5a). As expected we observe much less fault slip compared to the first two previous simulations (Figure 5b). However, the displacement recovery is bigger considering the smaller slippage distance in the treatment stage. When the frictional shear stress is still too high for the fault to have permanent slip, the two sides of the fault will undergo elastic slip. In this case, due to the increased static frictional coefficient and contact pressure, the maximum shear stress is increased that the two sides of the fault can not move far away and fast enough to reach the threshold for non-elastic slip and kinetic friction status for most of the simulation time. Therefore, the movement of the two sides remains mostly elastic and recoverable throughout the simulation due to their small magnitudes. This test shows that, if the friction force is held above a certain value (with a higher static frictional coefficient and a lower injection pressure), the fault slippage is very minimal and involves a significant portion of movements of both sides of the fault.

Conclusions

We developed a preliminary geomechanical model simulating the behaviour of a reverse fault under hydraulic pressure loading. A coupled hydro-mechanical FEM model is employed in this study to account for the dynamic friction–slip rate–fluid pressure relationship. By varying fluid pressure loading histories and frictional movement criteria, we investigated the possible slippage of a fault under various scenarios. The results show that the relationship between fault displacement and fluid injection pressure is not linear. This study shows the importance of using a transient coupled hydro-mechanical model in estimating fault reactivation due to hydraulic loading. The combined effects of kinetic friction and stick-slip phenomenon necessitate full coupling between fluid pressure propagation and friction coefficient changes. Steady-state or one-way–coupled simulation may provide misleading information regarding fault slip distance and corresponding earthquake magnitudes. We cannot assume that earthquake magnitude is proportional to fault area and final slip distance due to the fact that there might be a number of back andforth movements throughout the simulation. It is also desirable to explore the relationship between fault-slip rate and earthquake magnitude due to the fact that fluid flow in the fault can cause the fault to undergo very small pre-slip elastic displacement. More rock mechanical tests are required to further investigate the frictional, mechanical and hydraulic behaviours of faults to have a better understanding of hydraulically-driven fault slippage.

Acknowledgements

The authors would like to thanks AER for allowing the publication of this research.The authors also thank Dr. Yu Jeff Gu for insightful discussion regarding earthquake mechanisms.

References

Baisch, S., Vörös, R., Rothert, E., Stang, H., Jung, R., & Schellschmidt, R. (2010). A numerical model for fluid injection induced seismicity at Soultz-sous-Forêts. *International Journal of Rock Mechanics and Mining Sciences*, 47(3), p. 405-413.

Barton, N., Bandis, S., & Bakhtar, K. (1985). Strength, deformation and conductivity coupling of rock joints. *International Journal of Rock Mechanics and Mining Sciences & Geomechanics Abstracts,* 22(3), p. 121-140.

Brace, W. F. & Byerlee, J. D. (1966). Stick-slip as a mechanism for earthquakes. *Science*, *153*(3739), p. 990-992.

P.C. Carman. (1956) .Flow of gases through porous media. Butterworths, London.

Harris, R. A., & Simpson, R. W. (1998). Suppression of large earthquakes by stress shadows: A comparison of Coulomb and rate-and-state failure. Journal of Geophysical Research: Solid Earth, 103(B10), p. 24439-24451.

Griggs, D., & Handin, J. (1960). Observations on fracture and a hypothesis of earthquakes. Geological Society of America Memoirs, 79, p. 347-364.

Martins, J. A. C., Oden, J. T., & Simoes, F. M. F. (1990). A study of static and kinetic friction. *International Journal of Engineering Science*, *28*(1), p. 29-92.

Schmitt, D. R. (2014). Basic geomechanics for induced seismicity: A tutorial. CSEG RECORDER (Nov 2014), 39 (9).

Rutqvist, J., Rinaldi, A. P., Cappa, F., & Moridis, G. J. (2013). Modeling of fault reactivation and induced seismicity during hydraulic fracturing of shale-gas reservoirs. *Journal of Petroleum Science and Engineering*, 107, p. 31-44.

Zhao, X. P., and R. P. Young. (2009). Numerical simulation of seismicity induced by hydraulic fracturing in naturally fractured reservoirs. *SPE Annual Technical Conference and Exhibition*. Society of Petroleum Engineers.